Distinguishing electronic contributions of surface and sub-surface transition metal atoms in Ti-based MXenes

Yizhou Yang,[1] Kanit Hantanasirisakul,[1,2] Nathan C. Frey,[3] Babak Anasori,[1,2,4] Robert J. Green,[5,6] Paul C. Rogge,[1] Iradwikanari Waluyo,[7] Adrian Hunt,[7] Padraic Shafer,[8] Elke Arenholz,[8,9] Vivek B. Shenoy,[3] Yury Gogotsi,[1,2] and Steven J. May[1,*]

[1] Department of Materials Science and Engineering, Drexel University, Philadelphia, PA 19104, USA
[2] A.J. Drexel Nanomaterials Institute, Drexel University, Philadelphia, PA 19104, USA
[3] Department of Materials Science and Engineering, University of Pennsylvania, Philadelphia, PA 19104, USA
[4] Integrated Nanosystems Development Institute, Department of Mechanical and Energy Engineering, Purdue School of Engineering and Technology, Indiana University – Purdue University Indianapolis, Indianapolis, IN 46202, USA
[5] Department of Physics and Engineering Physics, University of Saskatchewan, Saskatoon, Saskatchewan, Canada S7N 5E2
[6] Stewart Blusson Quantum Matter Institute, University of British Columbia, Vancouver, British Columbia, Canada V6T 1Z4
[7] National Synchrotron Light Source II, Brookhaven National Laboratory, Upton, NY 11973, USA
[8] Advanced Light Source, Lawrence Berkeley National Laboratory, Berkeley, CA 94720, USA
[9] Cornell High Energy Synchrotron Source, Cornell University, Ithaca, NY 14853, USA
* smay@drexel.edu

Abstract

MXenes are a rapidly-expanding family of 2D transition metal carbides and nitrides that have attracted attention due to their excellent performance in applications ranging from energy storage to electromagnetic interference shielding. Numerous other electronic and magnetic properties have been computationally predicted, but not yet realized due to the experimental difficulty in obtaining uniform surface terminations (T_x), necessitating new design approaches for MXenes that are independent of surface groups. In this study, we distinguished the contributions of surface and sub-surface Ti atoms to the electronic structure of four Ti-based MXenes (Ti_2CT_x, $Ti_3C_2T_x$, $Cr_2TiC_2T_x$, and $Mo_2TiC_2T_x$) using soft x-ray absorption spectroscopy, revealing minimal changes in the spectral features between the parent MAX phase and its MXene when no surface Ti atoms are present in the MXene, such as $Mo_2TiC_2T_x$ and $Cr_2TiC_2T_x$. In contrast, for MXenes with surface Ti atoms, here $Ti_3C_2T_x$ and Ti_2CT_x, the Ti L-edge spectra are significantly modified compared to their parent MAX phase compounds. First principles calculations provide similar trends in the partial density of states derived from surface and interior Ti atoms, corroborating the spectroscopic measurements. These results reveal that electronic states derived from sub-surface M-site layers are largely unperturbed by the surface groups, indicating a relatively short length scale over which the T_x groups alter the nominal electron count associated with Ti atoms and suggesting that desired band features should be hosted by sub-surface M-sites that are electronically more robust than their surface M-site counterparts.

Keywords: MXene, x-ray absorption spectroscopy, electronic structure

1. Introduction

The large family of 2D materials known as MXenes[1-4] has attracted intense interest due to their suitability for solution processing, hydrophilic surfaces, metallic conduction, and versatility in hosting a range of intercalant ions and molecules leading to excellent performance in applications including electrodes for supercapacitors and batteries,[5-9] electromagnetic interference shielding,[10-14] and flexible antennae.[15, 16] The general chemical formula for MXenes is $M_{n+1}X_nT_x$, where M is an early transition metal, X is carbon or nitrogen, and T_x represents surface species such as $=O$, $-OH^-$, and $-F^-$. MXenes can consist of multiple elements on the M-site, either as random alloys or in ordered arrangements.[17-19] Synthesis of solid solution MXenes such as $(Ti_{0.5},Nb_{0.5})_2C$ and $(V_{0.5},Cr_{0.5})_2C$ with randomly-mixed transition metals on the M-site was reported in 2012.[20] More recently, ordered double-M MXenes ($M'_2M''C_2T_x$ or $M'_2M''_2C_3T_x$) were realized following the discovery of ordered Cr_2TiAlC_2 MAX phase, in which the Cr and Ti atoms occupy separate planes along the *c*-axis.[21] The expansion of MXenes into ordered double-M chemistries not only broadens the array of compositions that can be accessed but also provides two distinct M-sites – surface and interior positions – that may contribute differently to the functional properties.

The electronic properties of MXenes have been explored mainly through temperature-dependent resistivity measurements, spectroscopic methods, and density functional theory (DFT) calculations.[1, 2, 4, 17, 22-29] Much of this work has highlighted the effects of surface groups and intercalation on the macroscopic electronic behavior. Depending on processing conditions and post-synthesis annealing procedures, the ensemble resistivity (ρ) of the same nominal MXene compound film (stack of several 2D MXene flakes) can vary by orders of magnitude and $d\rho/dT$ can be either positive or negative. For example, transport measurements are often dominated by interflake hopping that is sensitive to interlayer spacing, intercalated molecules, and surface-bound groups as a result of the processing to convert MAX phases to MXenes.[27, 30-32] Moreover, instead of providing detailed unoccupied state information, resistivity only provides a narrow view of overall electronic structure near the Fermi level. Electron-based spectroscopies reveal that the electronic band structure of $Ti_3C_2T_x$ shifts during annealing in vacuum due to desorption of surface species. DFT has been used to predict many properties of MXenes including magnetic ordering, semiconductor band gaps, and the presence of topological band features in MXenes.[18, 33-49] However, these predictions strongly depend on the specific T_x groups used in the calculations, which due to practical limitations of DFT, such as the supercell size, are commonly performed with uniform surface terminations. However, MXenes are known to host complex, spatially inhomogeneous, and synthesis-dependent surface chemistries.[50]

While this previous body of work has demonstrated that surface T_x groups alter the electronic properties of MXenes, the extent to which these terminations modify the electronic behavior of all M-site-derived bands or just the surface-most M-site atoms is currently unknown. Clearly, a detailed and layer-resolved understanding of the impact of T_x groups is critically important for interpreting how and why the experimental properties of MXenes deviate from computational predictions. However, this issue has not yet been experimentally explored, largely owing to the difficulty in separating electronic contributions arising from distinct M-site layers within MXenes. For instance, resistivity experiments only provide information on the ensemble behaviour of all layers, with intrinsic electronic behavior often obscured by interflake hopping processes. However, newly realized ordered double-M MXenes provide a unique opportunity to tailor the location of Ti within the material, from solely occupying the surface layers in Ti_2CT_x to residing in the sub-surface layers in $Mo_2TiC_2T_x$, thus allowing for the interactions of the T_x groups with Ti layers to be systematically tuned. By applying an elementally-resolved probe of electronic structure to a systematically-selected set of Ti-containing MXenes, we provide a direct measure of the differing electronic contributions of surface and sub-surface Ti atoms in MXenes.

In this study, we take advantage of the elemental specificity offered by x-ray absorption spectroscopy (XAS) to measure the unoccupied electronic states derived from Ti atoms in Ti_2CT_x, $Ti_3C_2T_x$, $Mo_2TiC_2T_x$, and $Cr_2TiC_2T_x$ MXenes in comparison with their corresponding Al-containing MAX phases. We show that in Ti_2CT_x, which has all Ti atoms located on its surface, the Ti $L_{2,3}$-edge spectra exhibit significant changes upon conversion from Ti_2AlC MAX to the Ti_2CT_x MXene. In contrast, MXenes with only interior Ti atoms ($Mo_2TiC_2T_x$ and $Cr_2TiC_2T_x$) exhibit minimal spectral changes following transformation from their parent MAX phases (Mo_2TiAlC_2 and Cr_2TiAlC_2, respectively), which we attribute to decreased interaction strength between surface group and the interior transition metal. Additionally, we show the robustness of the sub-surface M-site contributions to the electronic structure through DFT calculations that reveal the T_x influence on Ti-derived bands is significantly decreased in $Mo_2TiC_2T_x$ (no surface Ti atoms) compared to Ti_2CT_x and $Ti_3C_2T_x$ (with surface Ti atoms). This work points to the importance of deriving desired electronic and magnetic function from sub-surface M-site layers, laying out an important design principle in the ongoing search for robust magnetic or topological behavior in MXenes.

2. Methods

2.1 Sample Preparation

Ti$_2$AlC MAX phase was synthesized following a protocol reported previously.[20] Ti$_2$CT$_x$ was produced by etching 2 g of the MAX powder in a mixture of LiF (3g, Alfa Aesar) and 9 M HCl (20 mL, Fisher) at 35 °C for 15 h. The mixture was washed with DI water in two 175 mL tubes and centrifuged at 3500 rpm for 5 min. The washing process was repeated 3-4 times until a dark supernatant was obtained. The dark supernatant was decanted and the sediment was transferred to a 50 mL tube and hand-shaken vigorously for 10 min. Finally, the mixture was centrifuged at 3500 rpm for 1 h and the supernatant was filtered over a porous membrane (3501 Coated PP, Celgard, USA). A free-standing film of Ti$_2$CT$_x$ was removed from the membrane right after all the solution passed through the membrane. The film was further dried in a vacuum desiccator and stored in an Ar-filled glovebox to avoid long exposure of the film to ambient air and resultant oxidation.

To synthesize Ti$_3$C$_2$T$_x$, 2 g of Ti$_3$AlC$_2$ (Materials Research Center, Ukraine) was etched in a premixed solution LiF (3g, Alfa Aesar) and 9 M HCl (20 mL, Fisher) at 35 °C for 24 h. The washing protocol was similar to that of Ti$_2$CT$_x$. The final supernatant was filtered over a porous membrane (3501 Coated PP, Celgard, USA). The film was dried on the filtration setup overnight and further dried in a vacuum desiccator.

Mo$_2$TiAlC$_2$ MAX phase was synthesized following a protocol reported elsewhere.[17] Mo, Ti, Al and graphite powders (all from Alfa Aesar, Ward Hill, MA) with a molar ratio of 2:1:1.1:2 were ball-milled for 18 h using zirconia balls in plastic jars. The powder mixtures were heated in covered alumina crucibles at 5 °C/min to 1600 °C and held for 4 h under argon. After cooling, the porous compacts were milled and sieved through a 400 mesh sieve, producing powders with a particle size < 38 μm. To synthesize Mo$_2$TiC$_2$T$_x$, 2 g of the MAX powder was added to 40 mL of 48-51% aqueous HF solution and stirred at 50 °C for 48 h. The mixture was washed with DI water in two 175 mL tubes for at least 5 times or until the pH of the supernatant was higher than 5. Then the powder was collected over a PVDF membrane (5 μm, Millipore). To delaminate Mo$_2$TiC$_2$T$_x$ powder, 1 g of the powder was stirred in 10 mL of tetrabutylammonium hydroxide (TBAOH) aqueous solution (48 wt%, Sigma Aldrich) for 12 h. The mixture was washed with DI water and centrifuged at 3500 rpm for 15 min. The washing process was repeated 3 times. After a pH of 7-8 was reached, the supernatant was decanted and the sediment was dispersed in 30 mL of DI water and bath-sonicated (2510, Branson) at 40 kHz for 30 min in a water-ice sonication bath under argon bubbling. The final solution was centrifuged at 3500 rpm for 30 min and the supernatant was filtered the same way as Ti$_2$CT$_x$.

Cr$_2$TiAlC$_2$ MAX phase was synthesized in our laboratory. To synthesize Cr$_2$TiC$_2$T$_x$, 2 g of the MAX powder was added to a pre-mixed etchant containing 50% HF, HCl, and DI water with a ratio of 2:3:5. The mixture was stirred at 35 °C for 42 h and washed in a similar way to Mo$_2$TiC$_2$T$_x$. To delaminate Cr$_2$TiC$_2$T$_x$, 2 g of the etched mixture was stirred in 20 mL of TBAOH (25% in water, Aldrich). The mixture was washed with DI water and centrifuged at 3500 rpm for 15 min. The washing process was repeated 3-4 times. After a pH of 7-8 was reached, the supernatant was decanted and the sediment was dispersed in 25 mL of DI water and probe-sonicated (Fisher Scientific model 505 Sonic Dismembrator) for 30 min in a water-ice sonication bath under argon bubbling.

The phase purity and compositions of all MXenes was verified by x-ray diffraction (XRD) and x-ray photoelectron spectroscopy (XPS) as shown in Figure S1 and S2 in the supporting information. XRD results show the 002 peaks of MXene phases are at lower 2θ position relative to their corresponding MAX phases, which indicates an expansion of the the *c*-axis parameter. The Al 2*p* region in the photoemission spectra obtained from each MXene suggest the Al atoms in the MAX phases are fully etched away, except that there is a negligible amount of Al left in the Cr$_2$TiC$_2$T$_x$ MXene after etching.

2.2 XAS measurement

$L_{2,3}$-edge XAS measurements were performed at National Synchrotron Light Source II (NSLS-II) beamline 23-ID-2 (IOS) and the Advanced Light Source (ALS) beamline 4.0.2. The Ti *L*-edge was measured between 450 eV to 480 eV with an energy step size of 0.1 eV. The spectra used in this study were collected in total electron yield mode. All XAS measurements were performed at room temperature and under ultra-high vacuum.

2.3 DFT Calculations

DFT calculations were performed using the Vienna Ab-Initio Simulation Package (VASP).[51] The Perdew−Burke−Ernzerhof (PBE)[52] exchange-correlation functional and projector augmented wave (PAW) pseudopotentials[53] were used for all calculations. Structural relaxations were performed with a 520 eV plane-wave basis cutoff and a 10 × 10 × 1 Γ centered k-point mesh until forces on each atom were converged to below 10^{-2} eV/Å. Total energies were converged to 10^{-8} eV and a dense 21 × 21 × 1 Γ centered k-point mesh was used for computing densities of states. Calculations for Cr$_2$TiC$_2$T$_x$ were performed with and without spin polarization and a Hubbard U parameter of 4 eV for Cr, following previous DFT predictions of magnetic ordering in functionalized Cr$_2$TiC$_2$

3

MXenes.[18, 54] The Ti *d*-orbital-derived projected density of states (PDOS) was not significantly affected with spin polarization, so non-spin polarized results are reported here.

3. Result and Discussion

In order to investigate the effects of the Ti site occupancy within the MXene layers, three types of MXenes were investigated: compounds with i) Ti atoms only in the surface (Ti_2CT_x), ii) Ti atoms in both the surface and the middle transition metal layer ($Ti_3C_2T_x$), and iii) Ti atoms residing in only the center M-site layer ($Mo_2TiC_2T_x$ and $Cr_2TiC_2T_x$). Schematics of these structures, along with their corresponding Al-containing parent MAX phases[55], are shown in Figure 1. When the Al layer is etched out from Ti_2AlC (Figure 1a), both layers of Ti in Ti_2CT_x are exposed to the surface terminations. Figure 1b shows that when the Al layer is selectively etched from Ti_3AlC_2, the remaining MXene contains three layers of Ti, the top and bottom surface layers are similar to the Ti layers in Ti_2CT_x, while the center Ti layer is not bonded to the surface terminations. In contrast, when the Al layer is etched away from Mo_2TiAlC_2 and Cr_2TiAlC_2 (Figure 1c), the only Ti layer in

the resulting MXenes is sandwiched by two MoC or CrC layers in the sub-surface M-sites and does not directly bond to the surface terminations. Therefore, comparison of these four compounds allows us to directly probe the role of surface and interior Ti atoms on the electronic structure. Here we note that the M-layers in ordered double-M MXenes are nominally fully ordered[17, 56], although studies quantifying the degree of ordering are currently limited.

In Figure 2, we present the Ti $L_{2,3}$-edge spectra for all MAX and MXene studied here. The spectral features arise from electronic transitions in which electrons are excited from the occupied Ti 2*p* core-level orbitals to unoccupied Ti 3*d* valence orbitals. The spectra contain both the L_3 (~ 453 - 463 eV) and L_2 (~ 463 - 473 eV) edges, which are a result of spin-orbit splitting of the *p*-orbitals producing distinct $2p_{1/2} \rightarrow 3d$ (L_2) and $2p_{3/2} \rightarrow 3d$ (L_3) transitions. The measured spectra are thus reflective of the unoccupied Ti 3*d* density of states, but do not map directly onto the DOS due to interactions with the core hole created upon excitation. The MXene spectra shown in Figure 2 are representative of spectra obtained from multiple samples at different locations on the samples.
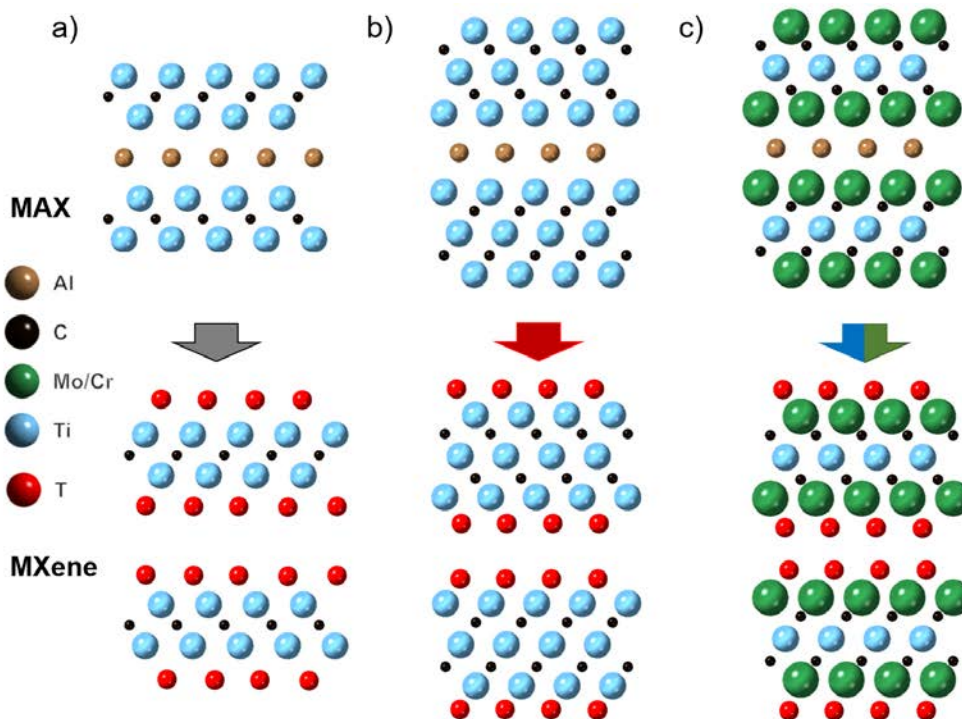
Figure 1: Schematic of MAX phases (top) and MXenes (bottom) investigated in this study. The MXenes are synthesized by removal of the Al layer in the MAX structures via chemical etching, a process that leaves behind a variety of surface species (T_x). (a) The conversion of Ti_2AlC to Ti_2CT_x MXene where all Ti atoms reside on surface sites, while (b) $Ti_3C_2T_x$ hosts both surface and interior Ti atoms, and (c) $Mo_2TiC_2T_x$ and $Cr_2TiC_2T_x$ exhibit ordered M-site arrangements, in which the Ti atoms reside in the middle transition metal layer. The T_x atoms (red) represent the mixed surface terminations (O^{2-}, F^-, OH^-).
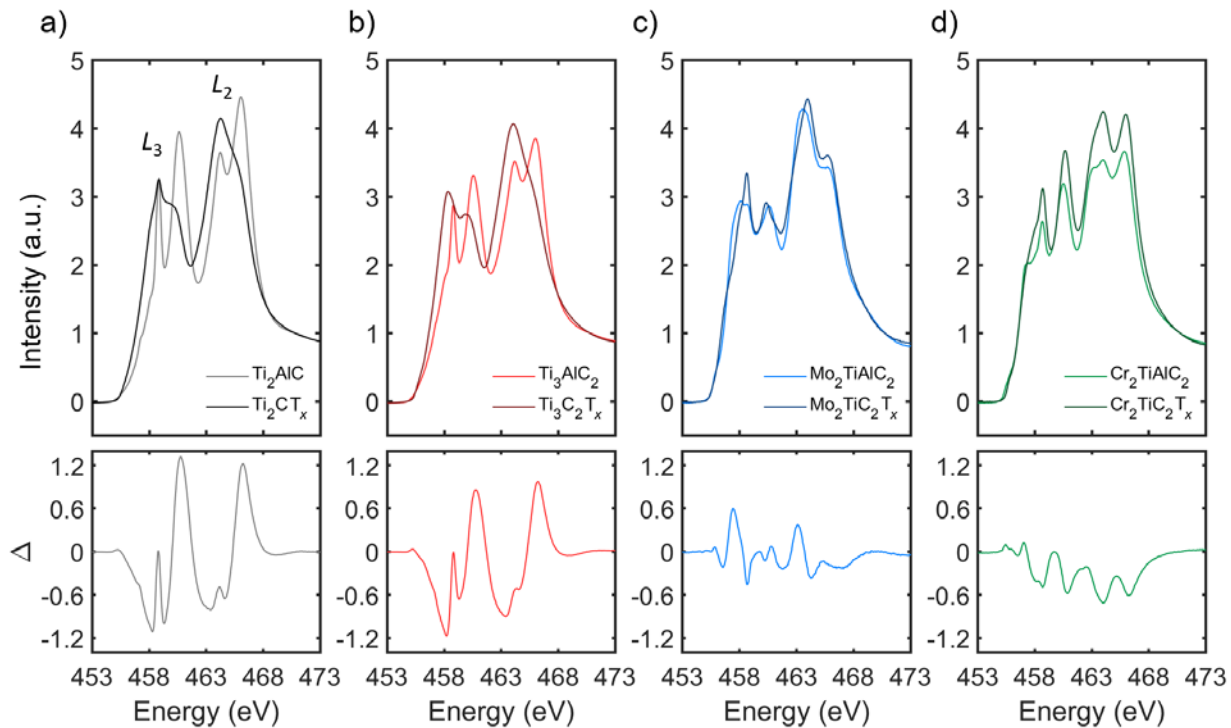
Figure 2: X-ray absorption spectra measured from (a) Ti_2CT_x and Ti_2AlC, (b) $Ti_3C_2T_x$ and Ti_3AlC_2, (c) $Mo_2TiC_2T_x$ and Mo_2TiAlC_2, and (d) $Cr_2TiC_2T_x$ and Cr_2TiAlC_2 at the Ti $L_{2,3}$-edge. In all data sets, MXene spectra are represented by the darker lines and the MAX spectra are represented by the lighter lines. Bottom panels display difference spectra (Δ) obtained by subtracting each MXene spectrum from its parent MAX spectrum.

Data over the wider spectral range from 450 eV to 480 eV are presented in Figure S3 in the Supporting Information. All the spectra shown in this study were normalized by subtracting the average pre-edge intensity (450 - 455 eV) from the raw spectra, and then by scaling the entire spectrum so that the post-edge absorption at 471 eV is set to unity. This post-edge energy was chosen to avoid the presence of single-hump-features between 473 eV to 480 eV which adversely affects the normalization process. The sample homogeneity and stability under x-ray flux was examined by measuring multiple positions on each of the samples. The x-ray absorption spectra are almost identical for the same sample at different positions as shown in Figure S4, indicating homogeneity of the samples. Also, each spot was measured twice resulting in unchanged spectra, which suggests that the samples do not degrade with exposure to the soft x-ray during the time of spectra collection (~15 minutes). Different batches of MXene samples were measured twice at NSLS-II and once at ALS. For all the MXene samples, the spectra are consistent across the three measurements, as shown in Figure S5, confirming the reproducibility of the MXene spectra.

Significant modifications to the spectral shapes are observed in Ti_2CT_x and $Ti_3C_2T_x$ with respect to their parent Ti_2AlC and Ti_3AlC_2 MAX phases. Single-M MXene spectra

(Figure 2a,b) have two noticeable changes from their parent MAX. First, the MXene spectral features are broadened with respect to the parent MAX phases. Second, the absorption peaks are shifted to lower energy in the MXene phase. In contrast, the spectra from the ordered double-M MXenes (Figure 2c,d) are very similar to that of their parent MAX phases. To further illustrate the Ti L-edge evolution from MAX to MXene, we present the difference spectra (Δ) as defined by subtracting the MXene spectra from the MAX spectra shown in the bottom panels of Figure 2. As all x-ray absorption spectra were normalized by the same process, the magnitude of the features in Δ can be directly compared between samples in order to quantify the relative spectral changes. Ti_2CT_x has the largest differences among all the samples, with features in the Δ spectrum approximately two times larger than that of the double-M MXenes.

We note that the difference spectra of Ti_2CT_x and $Ti_3C_2T_x$ show similar features (Figure 2a,b). When the Al layers are etched away, the bonding of the surface metal layer changes, from M-Al to M-T bonds. To further verify that the sub-surface metal layer (the center Ti layer here) is spectrally distinct from the surface metal atoms, we subtracted the Ti_2CT_x spectrum (containing only Ti surface atoms) multiplied by 2/3 from the $Ti_3C_2T_x$ spectrum (containing both surface and sub-surface Ti atoms), and the result is

shown in Figure S6 in the Supporting Information. Unlike the Ti_2CT_x and $Ti_3C_2T_x$ L_3-edge region, which has a broad peak with a shoulder feature, the difference spectrum shown in Figure S6 has a clear splitting in the L_3-edge. This L_3 splitting is also observed in the ordered double-M MXene spectra, suggesting that after eliminating the contribution from the surface transition metals through this spectrum subtraction process, the center Ti layer in $Ti_3C_2T_x$ is electronically similar to the Ti-derived bands in $Cr_2TiC_2T_x$ and $Mo_2TiC_2T_x$. This implies that the interactions between the center Ti layer in $M_3C_2T_x$ and the surface terminations are minimal compared to the M-T_x interactions in M_2CT_x MXene.

To further quantify the degree of changes to the electronic structure upon conversion from MAX to MXene, we calculated the integral of Δ^2 ($\int_{E_{pre-edge}}^{E_{post-edge}} \Delta^2 \, dE$) from the pre-edge to post-edge energy for each difference spectra as shown in Figure 3a. Ti_2CT_x has the largest integrated Δ^2 among the MXenes studied here, while the ordered double-M MXenes, in which the majority of Ti atoms reside in the sub-surface layers, have the smallest integrated Δ^2. This indicates that the spectral changes are more significant for the surface-derived bands than those derived from sub-surface metal atoms, and thus that the T_x groups have a minimal impact on the interior M-atoms compared to the surface M-atoms.

The relative concentration of d-electrons per Ti atoms can be inferred from the branching ratio which is defined as $\frac{\int I[L_3]}{\int (I[L_3]+I[L_2])} dE$, where I is the XAS intensity. Generally, in early transition metals, such as Ti, the branching ratio decreases as the d-orbital occupation decreases.[57-60] For example, in titanium oxides, the branching ratio decreases from 0.505 to 0.451 to 0.372 as electron count is decreased from d^2 to d^1 to d^0, as further discussed in the Supporting Information. To obtain accurate integrals within the L_2 and L_3 regions, an edge jump background was subtracted from the spectra prior to the branching ratio calculation based on Pearson *et al.*'s normalization method.[61] Figure 3b shows the differences in branching ratio between MAX and the corresponding MXenes. In all cases, the branching ratio decreases upon conversion of MAX to MXenes, indicating a decrease in the Ti electron count in MXenes compared to the parent MAX phases. Importantly, the decrease in branching ratio is the largest for MXenes with Ti on the surface sites and is the smallest in ordered double-M MXenes. This result is consistent with DFT calculations that routinely show a decrease in d-electron count in T_x-terminated MXenes compared to bare MXenes.[23] Additionally, previous XPS results on Ti_3AlC_2 and $Ti_3C_2T_x$ were interpreted in terms of a decreased electron count in the MXene relative to the corresponding MAX.
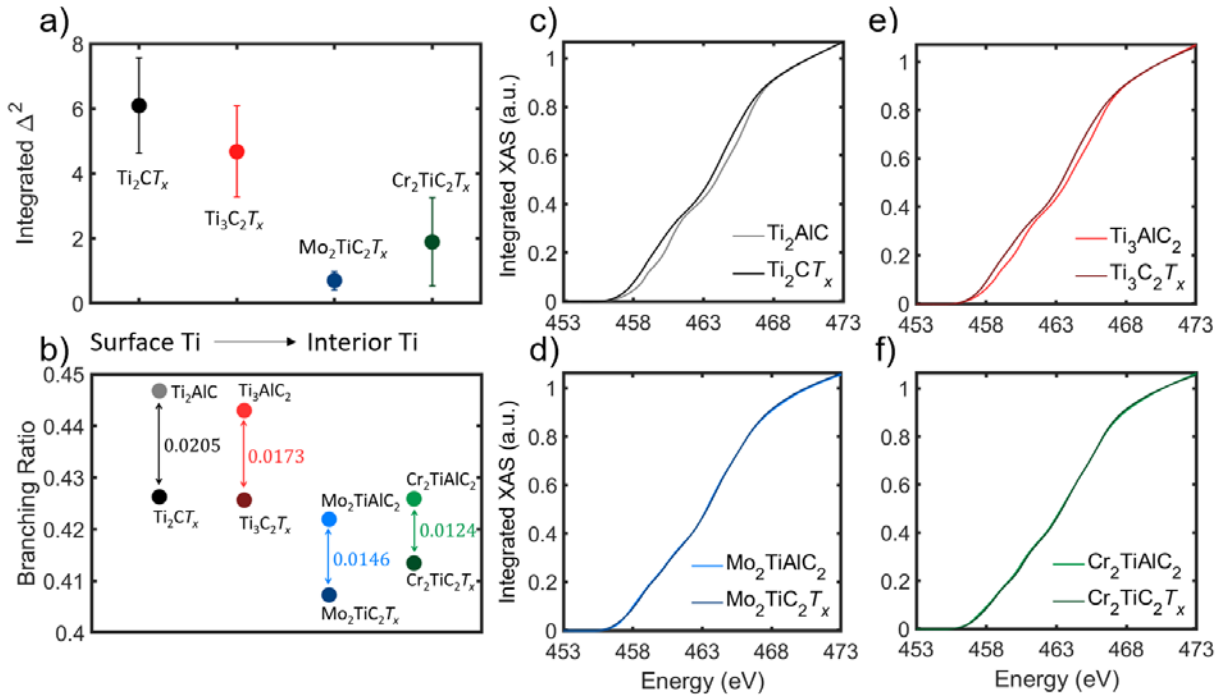

Figure 3: (a) Integrated Δ^2 (difference squared) provides a direct measurement of the differences between MAX and MXene spectra. Error bars are generated by systemically altering the 471 eV post-edge normalization position by ± 2 eV. (b) The branching ratio obtained from each spectrum. Panels (c-f) show the normalized integral of the x-ray absorption spectra for MXene and MAX compounds from pre-edge (455 eV) to post-edge (471 eV). Significant shifts in the leading absorption edge are only observed in the MXenes containing surface Ti.

Next, we consider the integrated XAS spectra as shown in Figure 3c-f. The spectra from MXenes that contain surface Ti atoms (Ti_2CT_x and $Ti_3C_2T_x$) exhibit a clear shift to lower energies after conversion from the MAX phases, while that of the MXenes with only interior Ti atoms ($Mo_2TiC_2T_x$ and $Cr_2TiC_2T_x$) do not (Figure 3e-f). These integrals are normalized to the total integrated spectral area up to the post-edge normalization energy (471 eV). In order to quantify the shift, we calculated the energy shift at every 10% of the normalized spectra integral. The average shift is -0.53 ± 0.16 eV for Ti_2CT_x, -0.47 ± 0.14 eV for $Ti_3C_2T_x$, 0.02 ± 0.05 eV for $Mo_2TiC_2T_x$, and -0.03 ± 0.04 eV for $Cr_2TiC_2T_x$, the error bars are calculated from the standard deviation of the shifts and do not take into account instrumental limitations. This shift to lower energies in Ti_2CT_x and $Ti_3C_2T_x$ can be seen in the difference spectra (Figure 2a,b) as the negative Δ feature at the onset of the L_3 absorption edge.

While a shift to lower energies in ionic compounds typically indicates reduction (an increased electron count of the cation), this interpretation is inconsistent with the branching ratio results. We note that the bonds in MXenes are highly covalent and thus an ionic-based interpretation of XAS based on isolated polyhedral units is likely inappropriate for metallic MXenes with delocalized electrons. Instead, we attribute the spectral shift to changes in the energetic positions of unoccupied Ti bands upon conversion from MAX to MXene, and not to reduction of Ti.

We computed elementally-resolved densities of states with DFT for relevant MXene and MAX compounds to better understand the origin of these spectral shifts. In Figure 4, we present the Ti d-orbital-derived PDOS above the Fermi level (E_F) for three types of MAX phases (Ti_2AlC, Ti_3AlC_2, and Cr_2TiAlC_2) and the corresponding O- and F-terminated MXenes. While OH-termination is also commonly observed in MXenes, the transition metal PDOS is not significantly different than that for isoelectronic F-termination[62-65], so we do not consider OH-termination here. We focus on the Ti-derived PDOS above E_F in these compounds as this is the region of the electronic structure probed by XAS.
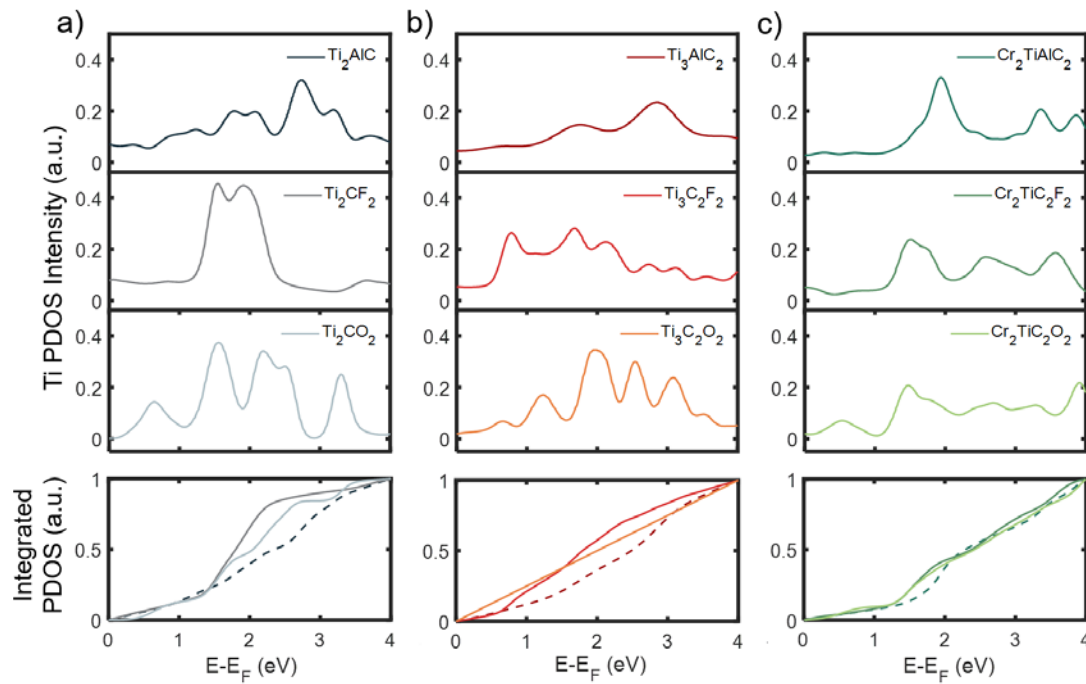
Figure 4: Ti d-orbital-derived unoccupied PDOS calculated for three MAX phases and the corresponding MXenes with Ti at different locations, (a) Ti on the surface in Ti_2AlC and Ti_2CT_x, (b) Ti on both surface and sub-surface sites in Ti_3AlC_2 and $Ti_3C_2T_x$, and (c) Ti at the sub-surface positions in Cr_2TiAlC_2 and $Cr_2TiC_2T_x$. Top panels are parent MAX phases, the second panels are MXenes with pure F termination, and the third panels are MXenes with pure O termination. The bottom panels show the normalized integral of PDOS for MAX (dashed line) and MXene compounds with pure F and O terminations.

MXenes with Ti layers on the surface (Figure 4a,b) displayed significant differences in the unoccupied electronic structure compared to the corresponding MAX phase, with the Ti PDOS of MXenes systematically shifting to lower energies. The middle two panels of Figure 4 display the calculated PDOS for the O- and F-terminated MXenes, revealing the emergence of new peaks in the PDOS and the shifting of states to lower energies as compared to the parent MAX compounds. The shifts to lower energy found for $Ti_3C_2T_x$ and Ti_2CT_x, which are readily visible in the normalized integration of PDOS shown in the bottom panels of Figure 4a,b, are qualitatively similar to the spectral shifts measured by XAS (Figure 3c-e). In contrast, the integrated PDOS for Cr_2TiAlC_2 and $Cr_2TiC_2T_x$ display a similar energy-dependence (Figure 4c) indicating that the electronic states of sub-surface Ti atoms in $Cr_2TiC_2T_x$ are largely unaffected by surface termination. Similar results were seen in Mo_2TiAlC_2 and $Mo_2TiC_2T_x$ (Figure S7).

Using Bader charge analysis, we obtain the change in the Ti atom charge between the MAX and MXene phases and confirm the proposed origin of the spectral shift. In Ti_2AlC, the average electron count is 2.8 e^-/Ti, while in the Ti_2CT_x MXenes, the average number of $3d$ electrons per Ti is 2.3-2.4 e^-/Ti for O- and F- terminations. Similarly, for the surface Ti atoms in Ti_3C_2, the Bader charge changes from 2.8 e^-/Ti (MAX) to 2.35 e^-/Ti (MXene). These changes suggest that the spectral shift can be attributed to changes in the positions of unoccupied Ti bands, rather than a reduction of Ti. However, the Bader charge on the sub-surface Ti atoms remains between 2.5-2.6 e^-/Ti for all MAX and MXene phases considered here, regardless of surface termination or composition. Detailed Bader charge changes for all transition metals can be found in Figure S8 These results support our interpretation of the changes to branching ratio and the origin of the absorption edge shifts upon conversion of MAX to MXene. Furthermore, the stability of the sub-surface Ti charge state and electronic states show the promise of engineering robust electronic, magnetic, and topological features in MXenes without control of the surface chemistry.

4. Conclusions

In summary, we have studied the contribution of Ti atoms residing at surface and interior M-site positions to the electronic structure of MXenes through XAS measurements and DFT calculations of MAX and MXene phases. $Mo_2TiC_2T_x$ and $Cr_2TiC_2T_x$, MXenes that contain only sub-surface Ti atoms, do not exhibit significant changes in the Ti L-edge spectra after conversion from the corresponding MAX phases. In contrast, Ti_2CT_x and $Ti_3C_2T_x$ exhibit significant spectral modifications due to the presence of T_x groups that interact with the surface Ti layers, consistent with previous

reports of surface terminations reducing the d-band electron count in these materials. The disparate electronic effects of T_x groups on surface and sub-surface M-sites is further confirmed through DFT calculations of unoccupied PDOS and Ti $3d$ electron densities. These results indicate that the electronic implications of the T_x groups are largely accommodated within the surface-most M-site layers and have much more limited impact on sub-surface M-site atoms. With these new insights, we propose a general design strategy to stabilize surface invariant properties in ordered double-M MXenes, wherein the interior M-site atoms are selected to host the desired electronic, magnetic, and topological functionalities.

Acknowledgements

References

[1] Naguib M, Kurtoglu M, Presser V, Lu J, Niu J, Heon M, Hultman L, Gogotsi Y and Barsoum M W 2011 *Adv. Mater.* **23** 4248-53.

[2] Naguib M, Mochalin V N, Barsoum M W and Gogotsi Y 2014 *Adv. Mater.* **26** 992-1005.

[3] Peng J H, Chen X Z, Ong W J, Zhao X J and Li N 2019 *Chem* **5** 18-50.

[4] Khazaei M, Mishra A, Venkataramanan N S, Singh A K and Yunoki S 2019 *Curr. Opin. Solid State Mater. Sci.* **23** 164-178.

[5] Boota M, Anasori B, Voigt C, Zhao M Q, Barsoum M W and Gogotsi Y 2016 *Adv. Mater.* **28** 1517-22.

[6] Naguib M, Come J, Dyatkin B, Presser V, Taberna P-L, Simon P, Barsoum M W and Gogotsi Y 2012 *Electrochim. Commun.* **16** 61-64.

[7] Wen Y, Rufford T E, Chen X, Li N, Lyu M, Dai L and Wang L 2017 *Nano Energy* **38** 368-376.

[8] Come J, Naguib M, Rozier P, Barsoum M W, Gogotsi Y, Taberna P-L, Morcrette M and Simon P 2012 *J. Electrochem. Soc.* **159** A1368-A1373.

[9] Anasori B, Lukatskaya M R and Gogotsi Y 2017 *Nat. Rev. Mater.* **2** 1-17.

[10] Shahzad F, Alhabeb M, Hatter C B, Anasori B, Man Hong S, Koo C M and Gogotsi Y 2016 *Science* **353** 1137-40.

[11] Feng W, Luo H, Wang Y, Zeng S, Deng L, Zhou X, Zhang H and Peng S 2018 *RSC Adv.* **8** 2398-2403.

[12] Han M, Yin X, Wu H, Hou Z, Song C, Li X, Zhang L and Cheng L 2016 *ACS Appl. Mater. Interfaces* **8** 21011-9.

[13] Liu J, Zhang H B, Sun R, Liu Y, Liu Z, Zhou A and Yu Z Z 2017 *Adv. Mater.* **29** 1702367.

[14] Cao M-S, Cai Y-Z, He P, Shu J-C, Cao W-Q and Yuan J 2019 *Chem. Eng. J.* **359** 1265-1302.

[15] Choi G, Shahzad F, Bahk Y-M, Jhon Y M, Park H, Alhabeb M, Anasori B, Kim D-S, Koo C M, Gogotsi Y and Seo M 2018 *Adv. Opt. Mater.* **6** 1701076.

[16] Sarycheva A, Polemi A, Liu Y, Dandekar K, Anasori B and Gogotsi Y 2018 *Sci. Adv.* **4** eaau0920.

[17] Anasori B, Xie Y, Beidaghi M, Lu J, Hosler B C, Hultman L, Kent P R C, Gogotsi Y and Barsoum M W 2015 *ACS Nano* **9** 9507.

[18] Sun W, Xie Y and Kent P R C 2018 *Nanoscale* **10** 11962-11968.

[19] Tao Q, Dahlqvist M, Lu J, Kota S, Meshkian R, Halim J, Palisaitis J, Hultman L, Barsoum M W, Persson P O Å and Rosen J 2017 *Nat. Commun.* **8** 14949.

[20] Naguib M, Mashtalir O, Carle J, Presser V, Lu J, Hultman L, Gogotsi Y and Barsoum M W 2012 *ACS Nano* **6** 1322-31.

[21] Liu Z, Zheng L, Sun L, Qian Y, Wang J and Li M 2014 *J. Am. Ceram. Soc.* **97** 67-69.

[22] Anasori B, Shi C, Moon E J, Xie Y, Voigt C A, Kent P R, May S J, Billinge S J, Barsoum M W and Gogotsi Y 2016 *Nanoscale Horiz.* **1** 227-234.

[23] Khazaei M, Ranjbar A, Arai M, Sasaki T and Yunoki S 2017 *J. Mater. Chem. C* **5** 2488-2503.

[24] Hantanasirisakul K and Gogotsi Y 2018 *Adv. Mater.* **30** e1804779.

[25] Zhan C, Naguib M, Lukatskaya M, Kent P R C, Gogotsi Y and Jiang D E 2018 *J. Phys. Chem. Lett.* **9** 1223-1228.

[26] Zhang N, Hong Y, Yazdanparast S and Zaeem M A 2018 *2D Mater.* **5** 045004.

[27] Hart J L, Hantanasirisakul K, Lang A C, Anasori B, Pinto D, Pivak Y, van Omme J T, May S J, Gogotsi Y and Taheri M L 2019 *Nat. Commun.* **10** 522.

[28] Yang Y, Umrao S, Lai S and Lee S 2017 *J. Phys. Chem. Lett.* **8** 859-865.

[29] Lai S, Jeon J, Jang S K, Xu J, Choi Y J, Park J-H, Hwang E and Lee S 2015 *Nanoscale* **7** 19390-19396.

[30] Wang Z, Kim H and Alshareef H N 2018 *Adv. Mater.* **30** 1706656.

[31] Hantanasirisakul K, Alhabeb M, Lipatov A, Maleski K, Anasori B, Salles P, Ieosakulrat C, Pakawatpanurut P, Sinitskii A, May S J and Gogotsi Y 2019 *Chem. Mater.* **31** 2941-2951.

[32] Halim J, Moon E J, Eklund P, Rosen J, Barsoum M W and Ouisse T 2018 *Phys. Rev. B* **98** 104202.

[33] Khazaei M, Ranjbar A, Arai M and Yunoki S 2016 *Phys. Rev. B* **94** 125152.

[34] Liang Y, Khazaei M, Ranjbar A, Arai M, Yunoki S, Kawazoe Y, Weng H and Fang Z 2017 *Phys. Rev. B* **96** 195414.

[35] Weng H, Ranjbar A, Liang Y, Song Z, Khazaei M, Yunoki S, Arai M, Kawazoe Y, Fang Z and Dai X 2015 *Phys. Rev. B* **92** 075436.

[36] Si C, Jin K H, Zhou J, Sun Z and Liu F 2016 *Nano Lett.* **16** 6584-6591.

[37] Balci E, Akkuş Ü Ö and Berber S 2018 *Appl. Phys. Lett.* **113** 083107.

[38] Balci E, Akkus U O and Berber S 2018 *J. Phys. Condens. Matter.* **30** 155501.

[39] Zhang X, Zhao X, Wu D, Jing Y and Zhou Z 2015 *Nanoscale* **7** 16020-5.

[40] Dong L, Kumar H, Anasori B, Gogotsi Y and Shenoy V B 2017 *J. Phys. Chem. Lett.* **8** 422-428.

[41] Tan T L, Jin H M, Sullivan M B, Anasori B and Gogotsi Y 2017 *ACS Nano* **11** 4407-4418.

[42] Frey N C, Kumar H, Anasori B, Gogotsi Y and Shenoy V B 2018 *ACS Nano* **12** 6319-6325.

[43] Yue Y 2017 *J. Magn. Magn. Mater.* **434** 164-168.

[44] Guo J, Legum B, Anasori B, Wang K, Lelyukh P, Gogotsi Y and Randall C A 2018 *Adv. Mater.* **30** e1801846.

[45] Sternik M and Wdowik U D 2018 *Phys. Chem. Chem. Phys.* **20** 7754-7763.

[46] Yang J, Luo X, Zhou X, Zhang S, Liu J, Xie Y, Lv L and Chen L 2017 *Comput. Mater. Sci.* **139** 313-319.

[47] Zhang Y, Xia W, Wu Y and Zhang P 2019 *Nanoscale* **11** 3993-4000.

[48] Guo Z, Zhou J, Zhu L and Sun Z 2016 *J. Mater. Chem. A* **4** 11446-11452.

[49] Si C, Zhou J and Sun Z 2015 *ACS Appl. Mater. Interfaces* **7** 17510-17515.

[50] Halim J, Cook K M, Naguib M, Eklund P, Gogotsi Y, Rosen J and Barsoum M W 2016 *Appl. Surf. Sci.* **362** 406-417.

[51] Kresse G and Furthmüller J 1996 *Phys. Rev. B* **54** 11169-11186.

[52] Perdew J P, Burke K and Ernzerhof M 1996 *Phys. Rev. Lett.* **77** 3865-3868.

[53] Kresse G and Joubert D 1999 *Phys. Rev. B* **59** 1758-1775.

[54] Yang J, Zhou X, Luo X, Zhang S and Chen L 2016 *Appl. Phys. Lett.* **109** 203109.

[55] Sokol M, Natu V, Kota S and Barsoum M W 2019 *Trends in Chem.* **1** 210-223.

[56] Liu Z, Wu E, Wang J, Qian Y, Xiang H, Li X, Jin Q, Sun G, Chen X, Wang J and Li M 2014 *Acta Mater.* **73** 186-193.

[57] Crocombette J P and Jollet F 1994 *J. Phys. Condens. Matter.* **6** 10811-10821.

[58] Wang Z L, Yin J S, Mo W D and Zhang Z J 1997 *J. Phys. Chem. B* **101** 6793-6798.

[59] Varela M, Oxley M, Luo W, Tao J, Watanabe M, Lupini A R, Pantelides S and Pennycook S 2009 *Phys. Rev. B* **79** 085117.

[60] Yedra L, Xuriguera E, Estrader M, Lopez-Ortega A, Baro M D, Nogues J, Roldan M, Varela M, Estrade S and Peiro F 2014 *Microsc. Microanal.* **20** 698-705.

[61] Pearson D H, Ahn C C and Fultz B 1993 *Phys. Rev. B: Condens. Matter.* **47** 8471-8478.

[62] Schultz T, Frey N C, Hantanasirisakul K, Park S, May S J, Shenoy V B, Gogotsi Y and Koch N 2019 *Chem. Mater.* **31** 6590-6597.

[63] Xie Y and Kent P R C 2013 *Phys. Rev. B* **87** 235441.

[64] Berdiyorov G R 2016 *AIP Adv.* **6** 055105.

[65] Bai Y, Zhou K, Srikanth N, Pang J H L, He X and Wang R 2016 *RSC Adv.* **6** 35731-35739.